dextran-filled diploic veins. These silhouettes represented the bony encasement of the diploic veins and the filling of the spongy diploe of cancellous bone, as shown in Fig. 2d, e, and f.

The area of the diploic veins increased gradually from 5 weeks to 45 weeks of age in Afdv (Fig. 3a; $p<0.01$) and Abedv (Fig. 3b; $p<0.01$).

Structural features and measurements of RBC velocity in the diploic veins

As shown in Fig. 4a, the FITC-dextran-filled diploic veins exhibited a unique pattern of microvasculature. The microvasculature was visualized as peculiarly shaped small vessels, which could be described as mega-capillaries or ectasia of microvessels (arrows). The larger veins were characterized by tortuosity and multiple ramifications with arborizing loops (arrowheads). The apical enlargements of the "hairpin-curved" vessels forming a hairpin head-like structure were observed within the bone encasement (Fig. 4b).

To characterize the hemodynamic features of these unique structures, we measured the blood flow in these regions of the diploic veins using FITC-labeled RBCs. As previously described, we used a high-speed camera (250 fps) for analysis of the microcirculation in the diploic veins. However, to show the FITC-labeled RBCs in the diploic vein clearly, we merged 10 images of the RBC movements captured sequentially at a rate of 30 frames/s in Fig. 5a.

When FITC-labeled RBCs were observed using video microscopy, we identified a group of high-speed RBCs at the entrance route to the diploic vein. At these entrance routes, the high-speed RBCs showed to have reached the diploic vein through the vessels in the basal periosteum of the cranial bone via the dura mater (Video data 1).

Then, the entrance route connected to the hairpin head of the diploic vein (Fig. 5a, long arrow; Fig. 5b, high-speed route; and Video data 2) and there was an abrupt decrease in the RBC flow velocity (short arrows). Furthermore, the RBC flowed only in the direction from the basal periosteum of the cranial bone to the diploic veins, and the velocity was significantly higher (5.5 ± 0.9 mm/s) than in the common parts (0.6 ± 0.2 mm/s) (Fig. 5c).

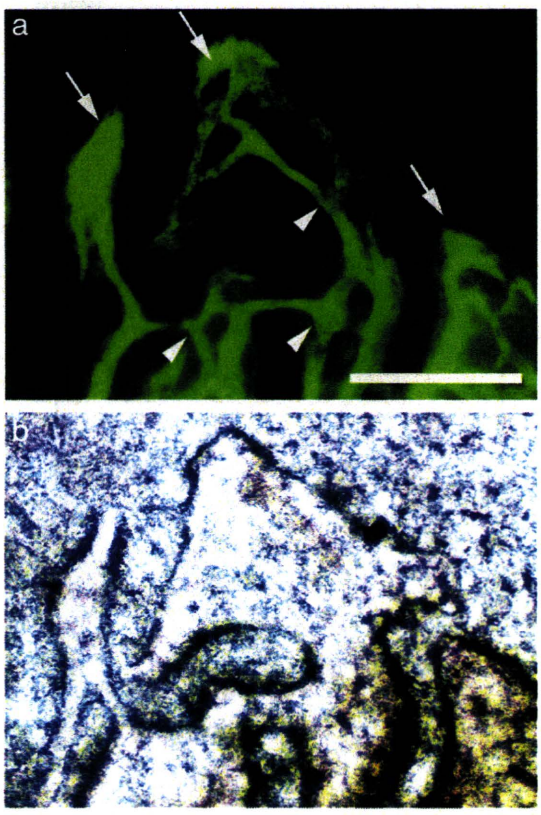

Fig. 4. (a) Vessel structure of the FITC-dextran-filled diploic veins with hairpin heads in a 16-week-old mouse. The microvasculature was visualized as peculiarly shaped small vessels, which could be described as mega-capillaries or ectasia of microvessels (arrows). The larger veins were characterized by tortuosity and multiple ramifications with arborizing loops (arrowheads). (b) The same area of the skull bone under transillumination showing the bony encasement of the diploic veins; scale bar, 250 μm.

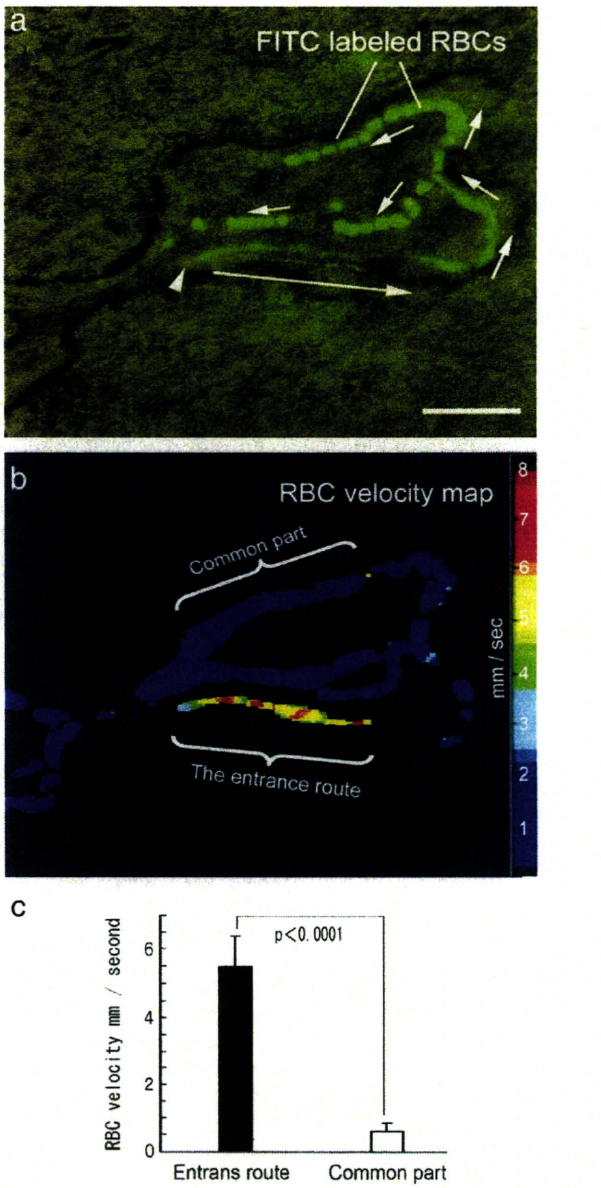

Fig. 5. (a) 10 sequential images of the RBC movements captured at a rate of 30 frames/s were merged to show the movement of the RBCs in the diploic veins. Scale bar, 100 μm. (b) RBC velocity map in the diploic veins. The RBCs travelled at high-speed at the narrow point of the diploic veins (arrowhead in a) and proceeded towards the top of the hairpin head (long arrow in a); thereafter, the RBC flow decelerated at the point indicated by short arrows. Color changes indicate velocity changes (scaled in the right bar). (c) The mean RBC velocity at the entrance route was 5.5 ± 0.9 mm/s (range, 7.1–4.0 mm/s; 23 RBCs in 6 animals; solid bar), and the velocity at the common part of the diploic veins was 0.6 ± 0.2 mm/s (range 1.3–0.2 mm/s; 56 RBCs in 6 animals; open bar). These values were significantly different ($p<0.0001$).

To indicate the relationship between the diploic veins and dural vessels clearly, we took pictures and made a movie file showing the FITC-dextran-filled diploic veins and dural vessel images obtained from a confocal microscope. These images clearly demonstrated the anastomoses of the diploic veins and dural vessels, when the focus gradually moved from the diploic veins towards the dural vessels (Fig. 6; Video data 3).

Discussion

In this study, the FITC-dextran-filled diploic veins represented the shape of the diploic veins *per se*, while the bone encasement of the diploic veins demarcated the structure of the bone encasement containing the diploic veins and the surrounding attachments. The age-dependent developmental pattern of the total areas of the FITC-dextran-filled diploic veins coincided with the age-dependent developmental pattern of the bone encasement of the diploic veins.

Communication between the intra-cranial circulation and the diploic veins was previously reported in an autopsy study of cadavers (Zenker and Kubik; 1996), but the details of the microcirculation at the diploic veins remained unclear. However, García-González et al. (2009) recently reported that the diploic veins drain into the cerebral sinuses in humans. Therefore, it is clear that the diploic veins connect with the dural vessels and the cerebral sinuses. Since the diploic veins are devoid of venous valves (Zenker and Kubik; 1996), the blood in these vessels can flow in both directions. However, under the conditions of this experiment, which used anesthetized normal mice, the direction of blood flow in the diploic veins was exclusively from the basal periosteum of the cranial bone to the diploic veins in all cases. These findings indicate that the blood flow originating from the intra-cranial circulation may reach the diploic veins via the dural vessels, and then drain into the cerebral sinuses. During this process, the blood temperature might be decreased as the blood passes through the diploic veins. Although this is only a hypothesis, it would be consistent with the previous hypothesis that the diploic veins may serve as a part of the brain-cooling system (Kunz and Iliadis, 2007).

Another important finding of the *in vivo* imaging in the present study was the identification of a group of high-speed RBCs at the

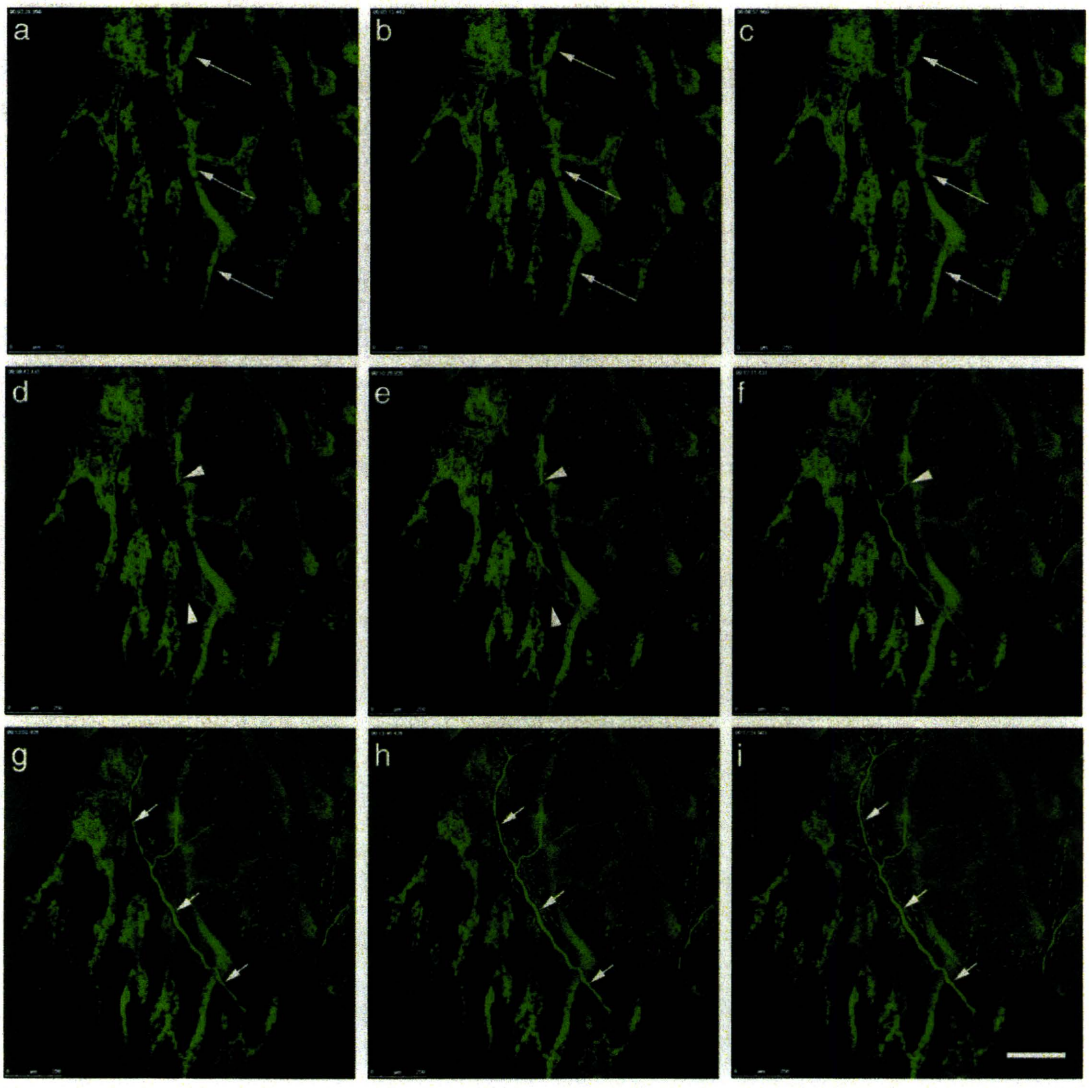

Fig. 6. The serial confocal sections taken through a FITC-dextran-filled parietal portion of the skull with the dura mater at 5 μm intervals for z-steps. The focus gradually moved from the diploic veins towards the dural vessels (a → i). The long arrow indicates the diploic veins (a, b, c), the arrowhead indicates the anastomoses of the diploic veins and dural vessels (d, e, f), and the short arrow indicates dural vessels (g, h, i). Scale bar, 250 μm.

entrance route to the diploic vein. The radicular veins have been reported to exhibit a narrowing structure at the points where they penetrate the dura mater (van der Kuip et al., 1999). Likewise, the narrowing structure of blood vessels appears to represent an entrance point of the diploic veins from the dural vessels, and the velocity of RBCs may reflect their high speed as they pass through these constricting passages.

The present study is the first to describe provide *in vivo* observations and analysis of these intra-extra circulatory communications. Our results should provide important clues toward a fuller understanding of diploic vein functions under certain pathophysiological states.

Supplementary materials related to this article can be found online at doi:10.1016/j.mvr.2010.11.004.

Conflict of interest statement

The authors have no conflicts of interest to declare.

Acknowledgments

This research was supported in part by Grants-in-Aid for Scientific Research (No. 21890250, to H. Toriumi and No. 19591005 to T. Shimizu) from the Ministry of Education, Culture, Sports, Science and Technology of Japan. The authors also thank the Otsuka Pharmacological Company for their financial support.

References

García-González, U., Cavalcanti, D.D., Agrawal, A., Gonzalez, L.F., Wallace, R.C., Spetzler, R.F., Preul, M.C., 2009. The diploic venous system: surgical anatomy and neurosurgical implications. Neurosurg. Focus 27, 1–11.

Hershkovitz, I., Greenwald, C., Rothschild, B.M., Latimer, B., Dutour, O., Jellema, L.M., Wish-Baratz, S., Pap, I., Leonetti, G., 1999. The elusive diploic veins: anthropological and anatomical perspective. Am. J. Phys. Anthropol. 108, 345–358.

Kunz, A.R., Iliadis, C., 2007. Hominid evolution of the arteriovenous system through the cranial base and its relevance for craniosynostosis. Childs Nerv. Syst. 12, 1367–1377.

Langer, K., 1877. Über Die Blutgefässe der Knochen des Schädeldaches und der harten Hirnhaut. Denkschr. K. Akad. Wiss. Wien. 37, 217–238.

Seylaz, J., Charbonné, R., Nanri, K., Von Euw, D., Borredon, J., Kacem, K., Méric, P., Pinard, E., 1999. Dynamic in vivo measurement of erythrocyte velocity and flow in capillaries and of microvessel diameter in the rat brain by confocal laser microscopy. J. Cereb. Blood Flow Metab. 19, 863–870.

Stenzel, E., 1954. Importance and use of the diploic veins in cranial roentgenography. Nervenarzt 25, 11–20.

Testut, L., 1921. Anatomie generale. In: Testut, L. (Ed.), Livre Premier Osteology. : Traite D' Anatomie Humaine, vol. 1. Octave Doin, Paris, pp. 1–60.

Tomita, M., Osada, T., Schiszler, I., Tomita, Y., Unekawa, M., Toriumi, H., Tanahashi, N., Suzuki, N., 2008. Automated method for tracking vast numbers of FITC-labeled RBCs in microvessels of rat brain *in vivo* using a high-speed confocal microscope system. Microcirculation 15, 163–174.

Tomita, Y., Kubis, N., Calando, Y., Tran Dinh, A., Méric, P., Seylaz, J., Pinard, E., 2005. Long-term in vivo investigation of mouse cerebral microcirculation by fluorescence confocal microscopy in the area of focal ischemia. J. Cereb. Blood Flow Metab. 25, 858–867.

Toriumi, H., Tomita, M., Tomita, Y., Osada, T., Unekawa, M., Shimizu, T., Suzuki, N., 2007. "Chestnut" (amaguri) method to visualize vessels in the dura and skull bone in mice. J. Cereb. Blood Flow Metab. 27 (Suppl. 1), 692 abstr.

Van der Kuip, M., Hoogland, P.V., Groen, R.J., 1999. Human radicular veins: regulation of venous reflux in the absence of valves. Anat. Rec. 254, 173–180.

Zenker, W., Kubik, S., 1996. A Brain cooling in humans—anatomical considerations. Anat. Embryol. Berl. 193, 1–13.

ARTICLE IN PRESS
YNIMG-08133; No. of pages: 10; 4C: 4, 5, 6, 7, 8
NeuroImage xxx (2011) xxx–xxx
Contents lists available at ScienceDirect
NeuroImage
journal homepage: www.elsevier.com/locate/ynimg

Oscillating neuro-capillary coupling during cortical spreading depression as observed by tracking of FITC-labeled RBCs in single capillaries

Minoru Tomita, Yutaka Tomita, Miyuki Unekawa, Haruki Toriumi, Norihiro Suzuki *

Department of Neurology, School of Medicine, Keio University, Tokyo, Japan

ARTICLE INFO

Article history:
Received 1 September 2010
Revised 25 February 2011
Accepted 28 February 2011
Available online xxxx

Keywords:
Capillary plasma viscosity
Cortical spreading depression
Neuro-capillary coupling
RBC tracking map
RBC in single capillary
Stunned neurons

ABSTRACT

Coupling between capillary red blood cell (RBC) movements and neuronal dysfunction during cortical spreading depression (CSD) was examined in rats by employing a high-speed camera laser-scanning confocal fluorescence microscope system in conjunction with our Matlab domain software (KEIO-IS2). Following microinjection of K^+ onto the surface of the brain, changes in electroencephalogram (EEG), DC potential and tissue optical density were all compatible with the occurrence of a transient spreading neuronal depression. RBC flow in single capillaries was not stationary. Unpredictable redistribution of RBCs at branches of capillaries was commonly observed, even though no change in diameter was apparent at the reported site of the capillary sphincter and no change of arteriolar-venule pressure difference was detected. There appeared to be a slow morphological change of astroglial endfeet. When local neurons were stunned transiently by K^+ injection, the velocity and oscillation frequency of RBCs flowing in nearby capillaries started to decrease. The flow in such capillaries was rectified, losing oscillatory components. Sluggish floating movements of RBCs in pertinent capillaries were visualized, with occasional full stops. When CSD subsided, RBC movements recovered to the original state. We postulate that neuronal depolarization blocks oscillatory signaling to local capillaries via low-shear plasma viscosity increases in the capillary channels, and a complex interaction between the RBC surface and the buffy coat on the capillary wall surface increases the capillary flow resistance. Then, when CSD subsides and oscillatory neuronal function is recovered, the normal physiological conditions are restored.

Introduction

The various flow control systems of cerebral vessels serve mainly to supply blood to the capillaries at levels sufficient to meet local neuronal requirements. RBC capillary flow behavior is especially important, since RBCs are the predominant oxygen carrier from the lung to the brain tissue. However, RBCs in blood do not behave like solutes, since their dimensions are of the same order as capillaries, so that their passage is constrained by local changes in viscosity, morphological transformation and so on. To visualize capillary flow in brain tissue *in vivo* at a depth of a few hundred micrometers below the pia mater, highly spatially-resolved two-photon microscopy (Chaigneau et al., 2003; Kleinfeld et al., 1998; Kleinfeld and Denk, 2000; Takano et al., 2007a; Takano et al., 2007b) has been employed, but rapid RBC movements in response to neuronal activation are difficult to examine because of the limited time resolution of this method. By employing a traditional intravital microscopic technique combined with novel use of fluorescein isothiocyanate (FITC)-labeled RBCs in the circulating blood, Biswal et al. observed low-frequency spontaneous oscillations in RBC capillary flow. After nitric oxide synthase inhibition, they found that the mean RBC velocity in the capillaries decreased to about half, but the 4–8 cpm (cycles per minute) frequency oscillations in velocity increased by about two-fold. They claimed that this, for the first time, provided direct evidence for low-frequency synchronous oscillations of RBC flow velocity in the cerebral capillary network (Biswal and Hudetz, 1996). However, the concept of capillary vasomotion was not new, since August Krogh had drawn attention to the influence of neuronal regulation on nearby capillary blood flow much earlier (Krogh, 1919). Furthermore, we had observed 4–6 cpm fluctuations in optical recordings of local cerebral blood volume (including arterioles, capillaries and venules) (Tomita et al., 1981) in cats. Introducing a confocal laser-scanning technique for intravital microscopy improved the spatial resolution (Seylaz et al., 1999; Villringer et al., 1994) and the velocity changes and even changes in the direction of flow of RBCs in capillaries could be traced.

Recently, the concept of the neurovascular unit, in which the activity of neurons modulates regional and local cerebral blood flow (CBF), has been proposed (del Zoppo, 2010). It is suggested that

Abbreviations: CBF, cerebral blood flow; CSD, cortical spreading depression; EEG, electroencephalogram; FITC, fluorescein isothiocyanate; fps, frames per second; NO, nitric oxide; OD, optical density; RBC, red blood cell; ROI, region of interest; SABP, systemic arterial blood pressure.

* Corresponding author at: Department of Neurology, School of Medicine, Keio University, 35 Shinanomachi, Shinjuku-ku, Tokyo 160–8582, Japan. Fax: +81 3 3353 1272.
E-mail address: nrsuzuki@sc.itc.keio.ac.jp (N. Suzuki).

1053-8119/$ – see front matter © 2011 Elsevier Inc. All rights reserved.
doi:10.1016/j.neuroimage.2011.02.078

neurons and microvessels bi-directionally communicate with each other, with the participation of the intervening astrocytes. However, it has been difficult to directly observe microvascular flow, astrocyte function and neuronal activity *in vivo* because of methodological limitations.

To examine microcirculation at the level of capillaries, we improved the time resolution of our method by developing a high-speed camera laser-scanning confocal fluorescence microscopy system (Tomita et al., 2008a; Unekawa et al., 2008). One of our findings was that the RBC velocity was often independent of upstream arteriolar blood flow or tissue perfusion in the surrounding microvasculature as measured with, for example, the tissue hemodilution technique (Schiszler et al., 2000). When local blood flow was dramatically increased by topical application of nitric oxide (NO) on the brain surface, the capillary RBC flow was unexpectedly rather decreased (Tomita et al., 2009a). Application of exogenous NO causes excessive oxygenation in the tissue (Yanamoto et al., 2003), which would be toxic to neurons (Tomita et al., 1994), and this apparently impeded capillary flow via unknown mechanisms. Severe hypocapnia is known to enhance the heterogeneity of brain capillary perfusion, indicating a potential disturbance of cerebral microcirculation (Vogel et al., 1996). Thus, capillary RBC flow seemed to be locally and actively controlled by allowing the entry of only a limited portion of the blood volume in the arteriole (which may serve as a reservoir) into the capillaries in response to neuronal requirements. Furthermore, we found that under physiological and pathological conditions, the left–right distribution of RBCs at a branching site of capillaries was complex and unpredictable, as if RBCs were sucked up by a discontinuous force from the capillary, even though it has no muscle cells and showed no appreciable change in diameter. Nakai et al. also observed left–right RBC distribution in a closed capillary loop and attributed it to a precapillary sphincter (Nakai et al., 1981), but we could not confirm the presence of such a sphincter. These observations are in conflict with the historical arteriolar stopcock theory (Mchedlishvili, 1986) of parallel passive capillary flow distribution. It is therefore of great interest to know whether or not the local capillary flow is regulated by neurons adjacent to the capillaries.

The aim of this study was to examine comprehensively the hypothesis that direct neuro-capillary coupling occurs, by using a high-speed camera laser-scanning confocal fluorescence microscope which can detect variations of RBC flow in single capillaries within a certain region of interest (ROI). First, control RBC movements in single capillaries of the cortical tissue were measured, and then changes in RBC movements during cortical spreading depression (CSD) were evaluated, to obtain insight into potential negative effects of neurons on RBC flow in adjacent capillaries.

Materials and methods

General procedures

Animals were used with the approval of the Animal Ethics Committee of Keio University (Tokyo, Japan), and all experimental procedures were in accordance with the university's guidelines for the care and use of laboratory animals. Male Wistar rats of 10–15 weeks old (mean body weight 326 ± 31 g) were anesthetized with urethane (1 g/kg ip and added as necessary). The methods of opening a skull window for the continuous recording of FITC-labeled RBCs in the cortical microvasculature and the techniques of image analysis were basically the same as those reported in the literature (Seylaz et al., 1999; Tomita et al., 2005b), except for the particulars of the high-speed camera, which will be discussed below. Two fine Ag–AgCl electrodes (tip diameter = 200 μm, EEG-5002Ag, Bio Research Center, Japan), used for measurements of both electroencephalogram (EEG; high frequency components) and DC potential (low frequency or DC components), were inserted at the posterior (proximal) and anterior (distal) edge of the cranial window (4 mm in diameter) made in the parieto-temporal cortex. The reference electrode was placed in the space between the skull-bone and the scalp. CSD was induced by intraparenchymal microinjection of 5 μl of KCl solution (0.3 M) into the cerebral cortex through a small hole bored on the posterior region of the cranial window while the DC potential was continuously monitored in the parieto-temporal area. Systemic arterial blood pressure (SABP) was continuously recorded through a femoral arterial catheter via a surgical strain-gage (MLT0670 and ML117, ADInstruments, Australia). Mean SABP was simply calculated as systolic pressure plus diastolic pressure divided by 2. A multi-channel recorder (PowerLab 8/30, ADInstruments, Australia) was used to obtain continuous recordings of the EEG and DC potential amplified with a preamplifier and amplifier (Model 4002 and EX1, Dagan, Minneapolis, USA).

In contrast to our previous experiments, endothelial cells were not stained *in vivo* with FITC-dextran to identify capillaries, since FITC-dextran not only stained the capillary wall, but also increased the background brightness and caused microvascular derangement. The observation of RBC single-tracking and the minimal staining arising from FITC-dextran that leaked slightly from RBCs were sufficient to visualize capillary walls adequately for the present purpose (Tomita et al., 2008a). A small amount of FITC-labeled RBC suspension which had been prepared beforehand (Seylaz et al., 1999) was injected into the femoral vein so that the final percentage of FITC-labeled RBCs per total RBCs in the circulating blood was approximately 0.4%. Astrocytes were stained *in vivo* by means of direct application of 50–100 μl of 100 μM sulforhodamine 101 (Sigma Chemical, St. Louis, MO, USA) on the brain surface (Nimmerjahn et al., 2004) while FITC-labeled RBCs were circulating in the microvasculature.

After confirmation of the appearance of the FITC-labeled RBCs in the microvessels in the cerebral cortex, continuous recording was commenced with a conventional high-resolution camera (30 frames per second (fps), HDR-CX7, Sony, Tokyo, Japan) to obtain colored video clips, which were used to analyze the relationship between the RBC movement changes and the changes in background darkness as an index of neuronal depolarization (Tomita et al., 2005a; Tomita et al., 2002). Video images of the brain surface were continuously recorded throughout all experiments except for short interruptions to record images with the high-speed video system at 500 fps (Fig. 1). Switching between the two video systems was achieved simply by opening or closing appropriate channels in the assembly.

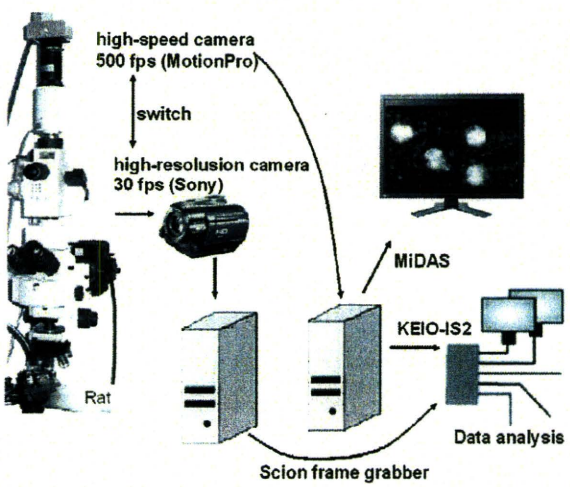

Fig. 1. Illustrative arrangement of the high-speed camera laser-scanning confocal fluorescence microscope assembly. Continuous video recording of the brain surface was made with a high-resolution camera at 30 fps (Sony). When necessary, the recording was interrupted and switched to a high-speed camera at 500 fps (MotionPro).

Please cite this article as: Tomita, M., et al., Oscillating neuro-capillary coupling during cortical spreading depression as observed by tracking of FITC-labeled RBCs in single capillaries, NeuroImage (2011), doi:10.1016/j.neuroimage.2011.02.078

High-speed video system

To visualize FITC-labeled RBCs, an argon laser ($\lambda = 488$, Melles Griot, Carlsbad, CA, USA), a multibeam confocal scanning unit (CSU22; Yokokawa, Tokyo, Japan), an image intensifier (C6653MOD-N; Hamamatsu Photonics, Hamamatsu, Japan) and a MotionPro high-speed camera (Model 500) with a digital imaging system using the MiDAS program file (RED-Lake, San Diego, CA, USA) were used. The objective lens (LU Plan EPI SLWD, 20× N.A. = 0.35, and 50× N.A. = 0.55; Nikon, Tokyo, Japan) provided a working distance from the objective lens to the brain surface of approximately 1.0 cm (except for the water immersion lens), which allowed convenient placement of electrodes for concomitant measurements of parameters such as EEG and DC potential, and also permitted the direct application of pharmacological agents to the brain surface. Images acquired with the confocal microscopic system after the appearance of intravenously administered FITC-labeled RBCs in the ROI had a narrow depth of focus in the region 80–100 μm below the brain surface (layer I). The confocal images with the high-speed camera system were stored in discrete video clips of up to 6000 frames each (24 s at 250 fps or 12 s at 500 fps) in an uncompressed AVI file format on terabyte-capacity hard disk drives.

Image-processing software KEIO-IS2

A selected video clip was transferred to a PC (Fig. 1) and analyzed off-line in a MATLAB (The Math Works, Inc., Natick, MA, USA) environment, using application software (KEIO-IS2) developed by one of the co-authors (I.S.) (Tomita et al., 2008a). The software makes no correction for movement along the *z*-axis, so that the RBC velocity is calculated as a two-dimensional value. It calculates the centroids of the recognized RBCs at the geometric center of the connected pixels, and positions them in the matrix automatically. The displacements of the centroids detected in subsequent frames were measured, and the velocities of individual RBCs in millimeter per second were calculated from the respective displacement distances of the centroids divided by the frame interval. The computer continues the calculations automatically for all labeled RBCs, numbering RBCs in the order of appearance, frame by frame for consecutive frames from the specified first frame to the specified last frame. The time required for the calculation of 1000 frames (4 s of image acquisition) was approximately 5 min with our PC (Sony VAIO, PCV 1140; Tokyo, Japan). After the calculation had been done, subsets of video clips containing features of interest were edited. For each subset, the computer automatically yielded three imaging maps: an RBC tracking map (T map) in which automatically numbered RBC tracks are shown in different colors, an RBC velocity map (V map) with a color scale, and an RBC number map (N map, or RBC Hct map). Parts of the RBC tracking map can be enlarged in a new window to analyze the details of RBC movements, and the relationships between individual RBCs that have passed through the same single capillaries can be examined repeatedly by selecting a small area on the T map.

In 5 rats, 0.2 ml of FITC-dextran (70 kDa, Sigma Chemical) solution (2.5 mg/ml) was administered via carotid artery, and motion pictures were obtained with the high-speed camera at 500 fps. Plasma flow was calculated by tracing the tip of the dextran dispersion.

The velocity data with identification numbers were then exported to a spreadsheet (Microsoft Excel) where the average velocities of all detected individual RBCs that moved in the ROI during the specified period were listed and classified into various categories for statistical treatment. Capillary data in this data subset were sorted in order of appearance and diagrammed (velocity diagram), or sorted in order of velocity magnitude for presentation as a histogram to illustrate the RBC velocity profile in the ROI during the specified period (velocity profile).

Highly magnified capillary images

To explore continuously RBC flow changes in the capillary network and redistribution at branching sites of the cortical microvasculature in association with CSD, while visualizing stained astroglial cells, 5 rat brain surfaces were observed with a high-magnification water immersion lens (Plan Fluor 60× W N.A. = 1.00; Nikon, Tokyo, Japan) placed on the exposed brain surface. FITC-labeled RBCs were injected into the femoral vein, and images were acquired with the high-resolution video camera to show the movements of FITC-labeled RBCs under epi-illumination with a halogen lamp (Model LH-M100CR-1; Hoya, Tokyo, Japan). The color motion pictures and changes in the background darkness, obtained by the subtraction technique as an index of neuronal depolarization, were analyzed off-line after the experiments.

Background darkness for the grading of CSD

As reported previously, high-K^+-induced CSD increases light transmission in neocortex slices submerged in flowing artificial CSF due to transient cell swelling with a concomitant reduction in extracellular volume (Anderson and Andrew, 2002). Repetitive elicitation of K^+-induced CSD was confirmed by the wave-ring spread of light transmission changes along the cerebral cortex from the site of the injection (Tomita et al., 2009b; Tomita et al., 2002), which is attributed to topographically chained membrane depolarization of brain cells and changes in local cerebral blood volume. To quantify the light transmission changes of the cortical tissue, optical density (OD) was calculated by subtracting the image of the frame zero from the image of any subsequent frame of a video clip taken at 30 fps and represented as relative scale. The sequential reflected-light pictures were analyzed by using a Scion LG-3 frame grabber card (Scion Corporation, MD, USA) to acquire images, which were automatically scaled logarithmically in brightness to 8-bit images. The changes of these images were compared on a 256 gray scale as an index of neuronal depolarization at the site. Background darkness represents the reciprocal of OD.

Results

General observations

The object of this study was to explore local RBC movements occurring in a limited area of the hemispheric cerebral cortex during the transition from physiological status to pathological K^+-induced CSD. Changes in physiological parameters observed here during CSD were broadly compatible with those previously reported by us (Osada et al., 2006; Tomita et al., 2005a; Tomita et al., 2008b; Tomita et al., 2002; Unekawa et al., 2009).

Fig. 2 illustrates the physiological parameter changes over recording periods of at least 1.7 min, in the order of occurrence. Topical microinjection of K^+ into the cortical tissue induced EEG flattening, negative deflection of DC potential, decrease in OD, and RBC disappearance from a limited area of the capillary network, with no change in SABP. The flattening of EEG as a target parameter of CSD, first reported by Leão (Leão, 1944), occurred during each episode of CSD, either immediately afterwards or apparently spontaneously in a repetitive manner. DC potential showed a negative deflection (-5.9 ± 2.6 mV; duration 115 ± 27 s; appearance 6.5 ± 3.2 times; spreading speed 3.5 ± 1.5 mm/min, mean ± SD, $n = 15$). Transient disappearance of RBCs from the capillary network for 3.3 ± 2.3 s ($n = 9$) and subsequent recovery of RBC flow were observed as reported by us previously (Tomita et al., 2008b); see also Fig. 13 below. The transient disappearance of all RBCs from a capillary network was quite rarely observed, although transient cessation of RBC flow often occurred in a single capillary. Some degree of RBC loss would likely result in local anoxia, which could be involved in the early stage of CSD, further aggravating the neuronal depolarization. The occurrence of tissue anoxia during CSD was indicated by the findings of Takano et al., who employed two-photon microscopic NADH imaging and oxygen sensor microelectrodes in live mouse cortex, and found that

Please cite this article as: Tomita, M., et al., Oscillating neuro-capillary coupling during cortical spreading depression as observed by tracking of FITC-labeled RBCs in single capillaries, NeuroImage (2011), doi:10.1016/j.neuroimage.2011.02.078

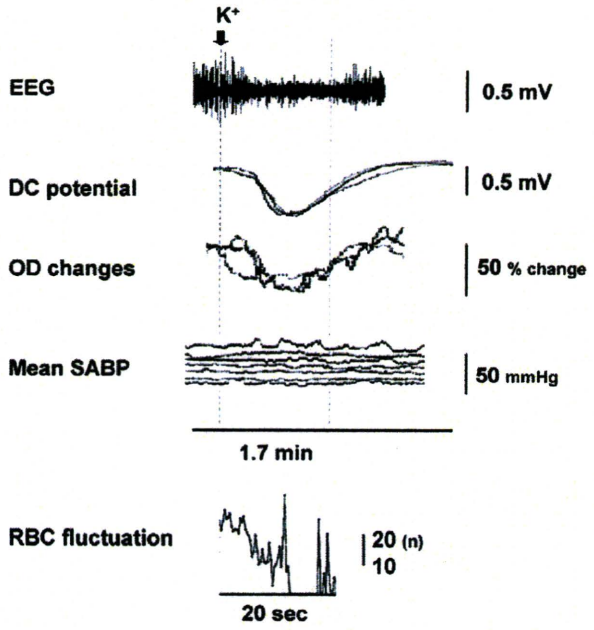

Fig. 2. Typical examples of physiological parameters. From the top: EEG (showing flattening), DC potential (showing a negative deflection), optical density (OD) changes of the local tissue in the background, mean SABP and fluctuating RBC velocity (showing disappearance from a limited area of capillary network). Recordings cover a period of approximately 2 min (see text for further explanation).

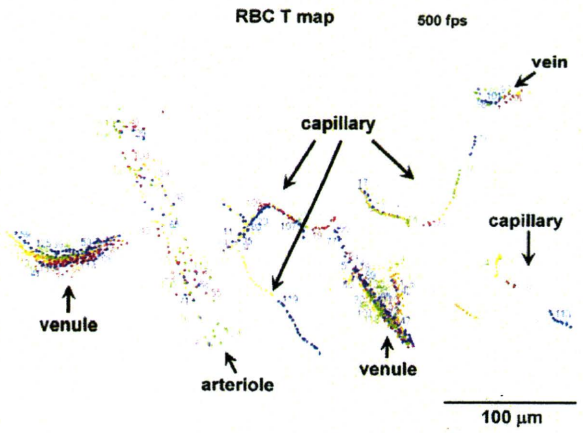

Fig. 4. A typical RBC tracking map (RBC T map) to show the locations of all RBCs labeled with FITC which were detected in the cerebral microvasculature in the ROI over a period of 4 s (2000 frames). Sequentially plotted dots and numbers in specific colors indicate frame-by-frame movements of RBCs in the microvasculature. The distance between dots of the same color in a sequence indicates the movement of each RBC during 1/500 s. The numbers indicate the order of appearance of RBCs represented by different colors. An off-line procedure was required to separate capillary components, since the figure contains all RBCs, including those that appeared in arterioles and venules.

CSD was linked to severe hypoxia and marked neuronal swelling that lasted up to several minutes (Takano et al., 2007b). Arterial blood pressure remained unchanged at 102–86 mmHg before and after the CSD propagation. The 7 parallel recording bars are continuous records of the average blood pressures from each of 7 rats; they show no change throughout the CSD episodes. These data support our idea that what we were observing during CSD was local events involving neurons in the cerebral cortex and associated RBC movement changes, not a part of a whole-body response.

Control view of flowing FITC-labeled RBCs, arterioles, capillaries, veins, and astroglia

A general view of the microvasculature in the cerebral cortex, with arterioles, capillaries and venules, as well as astroglial attachments, is shown in Fig. 3. In panel A, a branching arteriole and other vessels are viewed from above, illuminated with a laser beam at 488 nm. The arteriole is covered densely and seamlessly with bright brown-colored astroglial endfeet stained with sulforhodamine 101. From the surface of the endfeet, abundant processes extend into the tissue. FITC-labeled RBCs flowing in this arteriole are invisible since they run too fast to be captured with the low-speed camera (i.e., they are not captured in successive frames, and so cannot be recognized by the computer). No

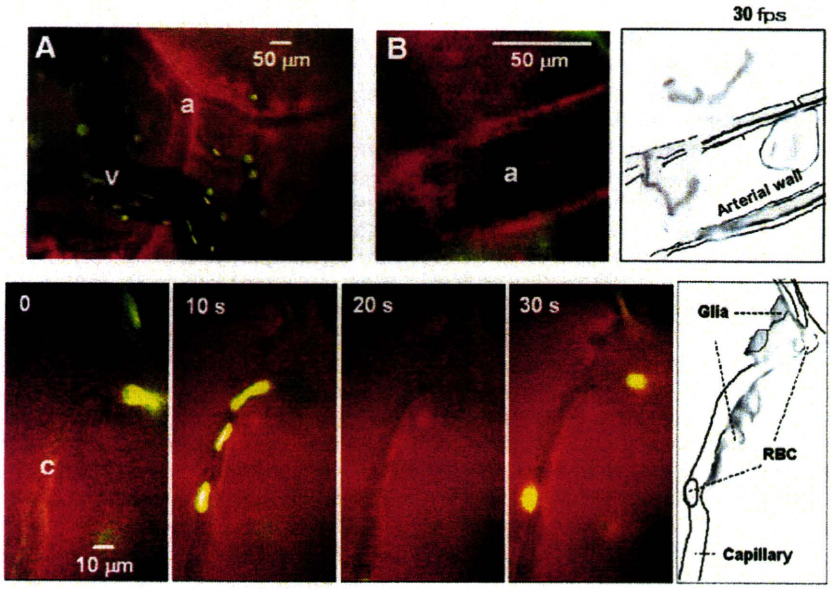

Fig. 3. General view of the brain surface microvasculature (a: arteriole, v: vein and venules, and c: capillary) and sulforhodamine 101-stained astroglial elements surrounding the cerebral vessels. In the right panels astroglial elements (soma and endfeet) are retouched in gray. FITC-labeled RBCs are seen in yellow. Color microphotographs were taken from frames of a video recording.

Please cite this article as: Tomita, M., et al., Oscillating neuro-capillary coupling during cortical spreading depression as observed by tracking of FITC-labeled RBCs in single capillaries, NeuroImage (2011), doi:10.1016/j.neuroimage.2011.02.078

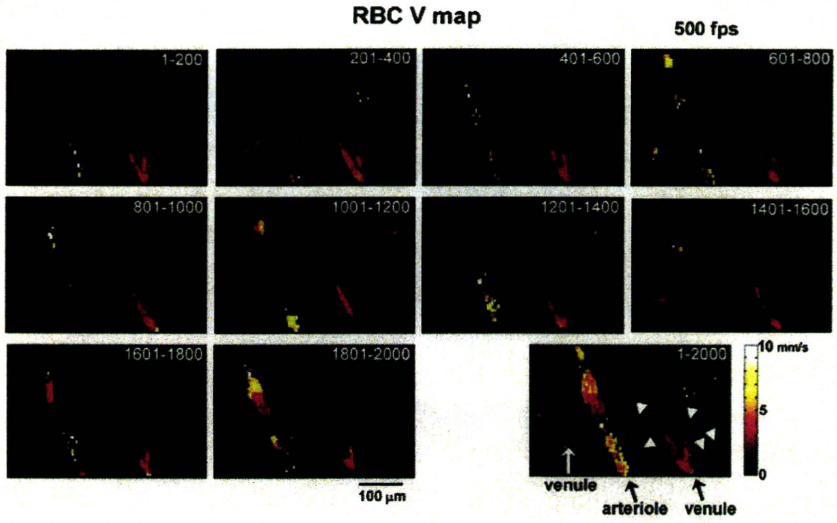

Fig. 5. Sequential RBC velocity (V) maps in a capillary network, 0.4 s apart. These maps were obtained from the identical ROI of the same rat as Fig. 4. Capillaries are shown by white arrowheads. Note the color heterogeneity, which represents different speeds of the same RBC in a single capillary (ranging from 0.33 to 2.60 mm/s), in an arteriole (ranging from 3.44 to 8.22 mm/s) and in venules (ranging from 1.27 to 4.52 mm/s).

attachments of astroglial elements to the vein are seen. RBCs in the vein are clearly visible in yellow color; some have a round shape and others are rather elongated. Panel B shows a longitudinal section of an arteriole of approximately 50 μm in diameter. There is a thick layer of astroglial endfeet colored brown and incompletely stained endothelial layers in green constituting the glio-vascular interface, where the Virchow–Robin space must exist. Because of the poor spatial resolution, we carefully illustrated the images and surmised a broad structural interrelationship between astroglial elements and the arteriole in which astroglia form a complete, thinly spread, continuous covering on the arteriolar surface, with a holding-type or synaptic-type *en face* contact with the vessel wall, as roughly illustrated in the right panel of the upper row. The lower row of Fig. 3 shows the interrelationship between a single capillary, glial endfeet and RBC movements at intervals of 10 s. There seem to be scanty synaptic-type or holding-type attachments of astroglial endfeet on the capillary surface. However, it should be noted that the absence of a brown-colored sheath around capillaries does not necessarily imply the absence of "membrane limitans gliae superficialis," as observed by electron-microscopy (Wolf, 1970). It seems likely that the astroglial endfeet layer covering capillaries would be too thin to hold the staining material.

Control RBC movements as viewed with high-speed video

As mentioned before, when FITC-labeled RBCs were injected into the circulating blood, they appeared in the cerebral microvasculature as bright circles against a dark background with the high-speed camera laser-scanning confocal fluorescence microscope. The program identified the vast number of RBCs as above-threshold light intensity features (Fig. 1), recognized their positions (centroids) in *x*–*y* coordinates frame by frame for the selected number of frames, and stored the data in the PC (Supplemental movie 1). Fig. 4 shows all RBCs that were detected in the visual field for 2000 frames (4 s). This map represents the fundamental data for this study. The numbers on the map define the order of appearance of RBCs, shown in different colors. From the data, the velocities of all RBCs were calculated based

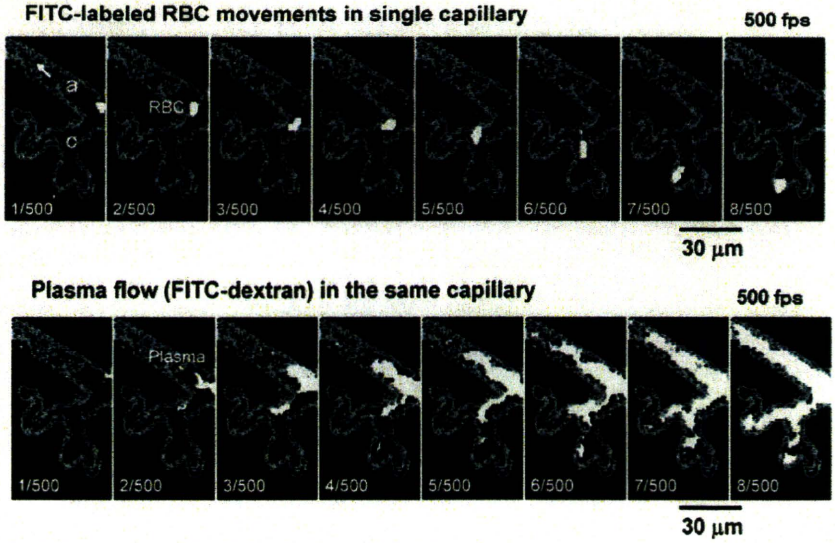

Fig. 6. To show RBC flow at 500 fps (top) in an arteriole (a) and a single capillary (c) and plasma flow (bottom) after intra-carotid injection of FITC-dextran. The frame intervals are 1/500 s (see text for further explanation).

Please cite this article as: Tomita, M., et al., Oscillating neuro-capillary coupling during cortical spreading depression as observed by tracking of FITC-labeled RBCs in single capillaries, NeuroImage (2011), doi:10.1016/j.neuroimage.2011.02.078

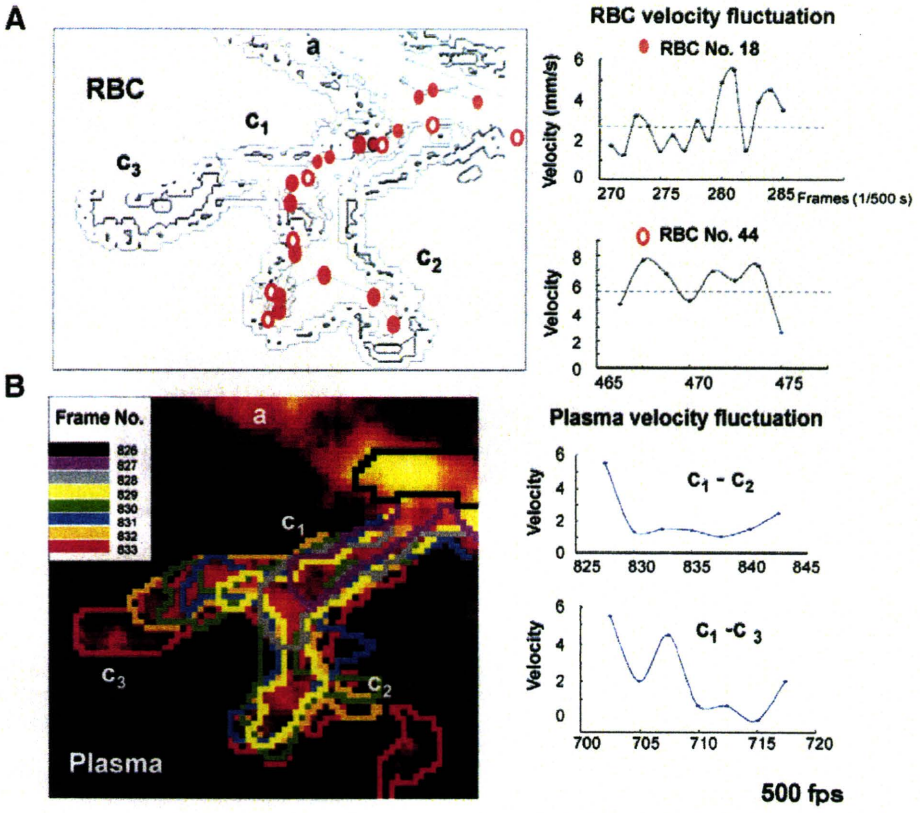

Fig. 7. More comprehensive analysis of the data shown in Fig. 6. Movements of two RBCs (A) in a specified period occurred in the capillary c2. In (B), contour changes of FITC-dextran were traced every 1/500 s in different colors, showing that a very variable diffusion process occurs at the boundary. The right panels of the two columns show the velocities of RBCs and plasma plotted against time in seconds. The synchronous fluctuations suggest that very complex vasomotion was occurring in the capillaries, which lack muscle cells.

on the displacement distance (μm) per frame multiplied by the frame rate (500 per second in this case), affording a velocity map (V map), and a topographical RBC number map for a specified period (RBC N map). Off-line analysis was required to separate RBCs in capillaries, since the figure contained all RBCs appearing even in arterioles and veins, and the computer cannot discriminate the vessels. Capillaries were identified by comparing the obtained maps and a movie recorded with a conventional video system. Fig. 5 is the V map of

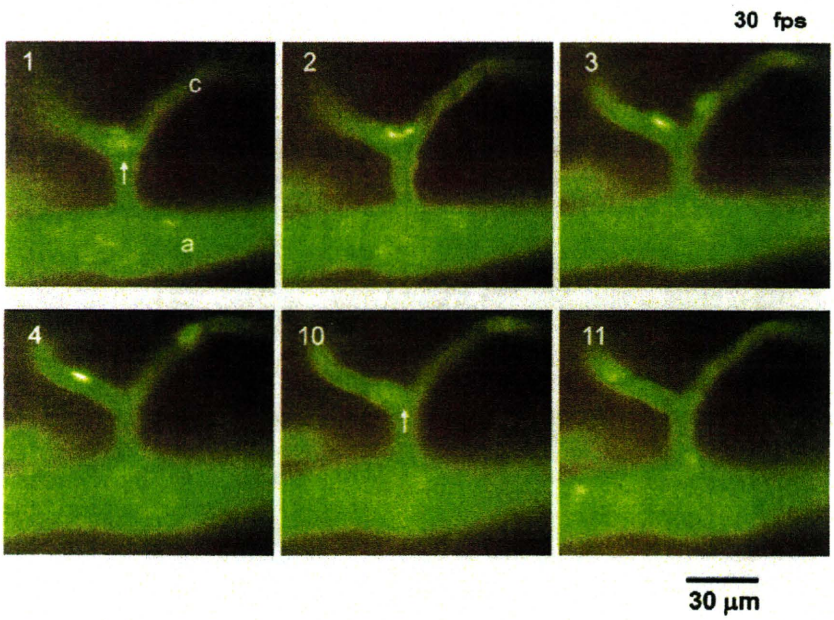

Fig. 8. Unpredictable left–right distribution of RBCs at a capillary branch. Two RBCs at the point of bifurcation separated and moved in opposite directions at frames 1, 2, 3 and 4 (30 fps) in the absence of any detectable change in diameter of capillary. Another RBC came at frame 10 and proceeded to the left capillary, again without any apparent change in diameter. These results seem inconsistent with the involvement of a putative capillary sphincter.

Please cite this article as: Tomita, M., et al., Oscillating neuro-capillary coupling during cortical spreading depression as observed by tracking of FITC-labeled RBCs in single capillaries, NeuroImage (2011), doi:10.1016/j.neuroimage.2011.02.078

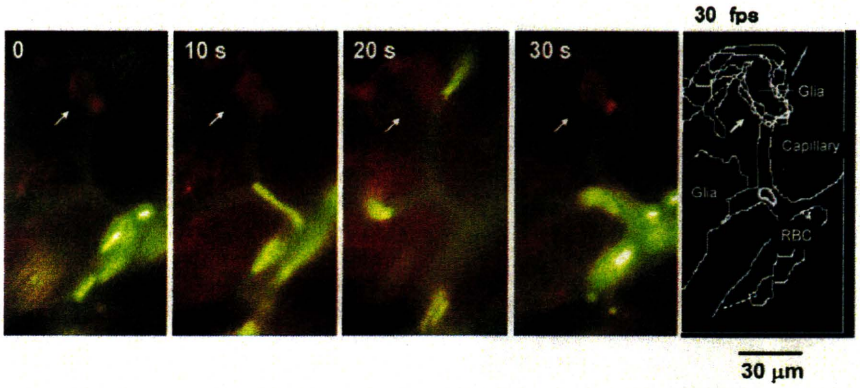

Fig. 9. Morphological changes of astroglial soma and endfeet over 30 s. An illustration of the cumulative morphological changes of the astroglial elements is shown in the right panel (arrow).

RBCs in microvessels obtained from the same motion picture as used for Fig. 4, showing the time-to-time changes in velocity of RBCs in a limited region, in sequences of 200 frames each, i.e., 1–200 (0.4 s), 201–400 (0.4 s), 401–600 (0.4 s).....1801–2000 (0.4 s). It should be noted that movements of RBCs are heterogeneous, not stationary, presumably reflecting local neuronal requirements, in line with previous reports that RBC flow in single capillaries continuously fluctuated within a limited range in rats and mice (Unekawa et al., 2008; Unekawa et al., 2010).

Fig. 6 shows a capillary in which an RBC is moving at intervals of 1/500 s in the upper row, together with plasma flow traced with FITC-dextran in the same capillary, on the same time scale. Note that plasma flow was also heterogeneous; indeed, the calculation of average plasma velocity was difficult because parts of the diffusion front moved faster while others moved slower, as analyzed in Fig. 7. In the lower panel, contours of plasma dispersion are traced at every 1/500 s. Both RBC flow and plasma flow showed rather high-frequency fluctuations (see the right panels). Evaluation with KEIO-IS2 yielded a value of RBC velocity in single capillaries of 2.00 ± 1.56 mm/s (mean $\pm$ SD, $n = 5$, at 500 fps) whereas a somewhat lower velocity of 1.80 ± 2.01 mm/s (mean $\pm$ SD, $n = 5$) was obtained for plasma propagation in the identical capillaries. Chronological plots of sequential RBC and plasma velocities revealed high-frequency fluctuation in 2 capillaries. These observations may contribute to efforts to understand the hemodynamic mechanisms of RBC flow in capillaries.

RBC distribution at capillary branching sites was simply unpredictable. Fig. 8 shows the left–right distribution of RBCs at a capillary branch. Two RBCs reached the branch at the first frame, separated, and moved off in opposite directions at the 2nd, 3rd and 4th frames (30 fps). There was no detectable change in the diameter of the capillary. At the 10th frame, another RBC arrived at the branch and proceeded into the left capillary, again without any apparent change in the diameter of the capillary. There was no indication of any role of a capillary sphincter, if such a structure exists (Nakai et al., 1981), leaving open the possibility that a transient plasma viscosity change directs RBCs to the pertinent capillary. Fig. 9 illustrates the slow morphological changes of astroglial endfeet, which covered a branch of the capillary at the periphery, every 10 s. RBCs, stained yellow, appeared elongated in the 30 fps video images. However, no direct correlation between the morphological changes and RBC velocity was apparent, although this phenomenon might reasonably have been expected.

RBC movements during CSD

RBC movements in single capillaries during CSD elicited by K^+ microinjection were observed to decrease gradually, with or without an initial transient increase, employing the same apparatus as used for the control study, except for the use of slow-speed video for the estimation of background darkness and the detection of slowing RBCs. The RBC velocity decreased in a fluctuating fashion and finally stopped at 6 min after the onset of CSD in this case while in other cases, RBCs disappeared from the local capillary network (Fig. 10 upper images and Supplemental movie 2). We found that RBC velocity decreased to nearly 0 in 5 out of 10 rats, and reversed RBC flow was seen in 3 out of 10 rats. Increasing neuronal depolarization during CSD was estimated from the darkness of the tissue background. However, there seemed to be some discrepancy: RBC flow tended to be preserved even after

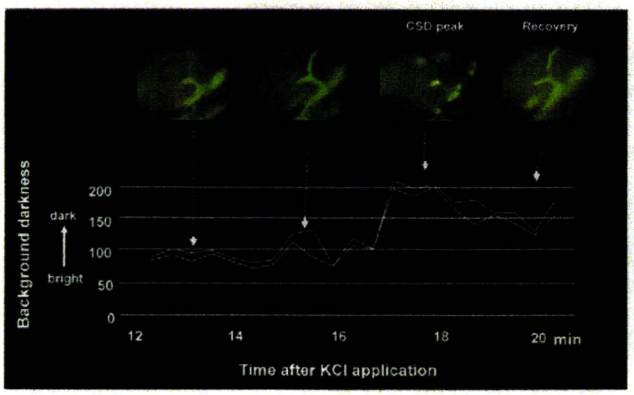

Fig. 10. Background darkness (neuronal depolarization) changes and sample images showing associated RBC movements. In this particular case, there seemed to be a slight discrepancy between the two processes, as the background darkening started before RBC flow decrease became detectable 14 min after KCl application.

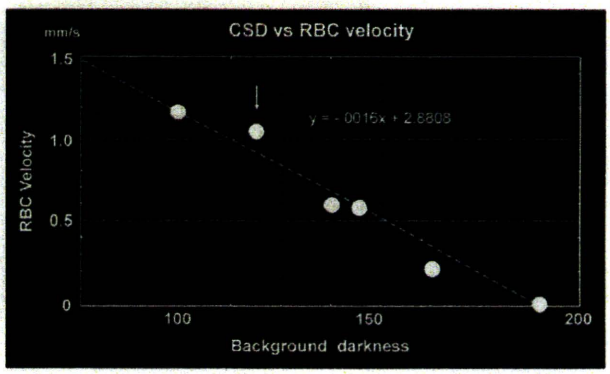

Fig. 11. Linear relationship between changes of tissue background darkness produced by neuronal depolarization and RBC velocity. Again, slowing of RBC flow (arrow) was slightly delayed compared with the start of background darkening.

Please cite this article as: Tomita, M., et al., Oscillating neuro-capillary coupling during cortical spreading depression as observed by tracking of FITC-labeled RBCs in single capillaries, NeuroImage (2011), doi:10.1016/j.neuroimage.2011.02.078

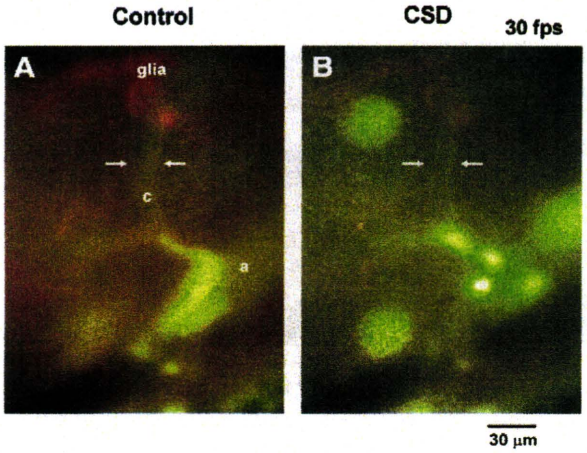

Fig. 12. No change in diameter of capillary occurred in the control period or during CSD, when the RBC velocity in the capillary decreased to less than 1/3 of the control value.

the background darkness started to decrease at 4 min. Such a lag time was often observed (Fig. 10), implying that the intrinsic neuronal depolarization occurred first, followed by a vascular event which was reflected in the change of RBC movements. A linear relationship between the darkness in arbitrary units and RBC velocity was confirmed, as shown in Fig. 11. As indicated by arrows in Fig. 12, there was no detectable change in the diameter of single capillaries between the control state and during CSD. The mechanism of the local slowing-down of RBC velocities was further examined in highly magnified capillaries during CSD passage. Fig. 13 and Supplemental movie 3 show RBCs moving slowly in viscous plasma during the peak of a CSD episode. At time 0, two RBCs were flowing through a capillary channel connecting an arteriole (a: lower) to a venule (v: upper). While the velocities of RBCs in both the arteriole and venule appeared to be rather well maintained, as estimated from RBC elongation, due probably to persisting flows in these vessels, in this short channel the RBC flow became extremely slow. In this sluggish flow, round RBCs in a single capillary (c) showed oscillating motion with occasional stagnation at certain spots, and finally disappeared at 4 or 5 s into the collecting venule. It should be noted that the capillary plasma appeared to be very sludgy and viscous, containing amorphous materials. The buffy coat on the internal surface of the capillary wall appeared to be thickened, continuing to or connecting with the intraluminal amorphous materials. In short, the apparent hemorheological changes were observed to occur in the capillary channels only, and not in inlet or outlet vessels.

Discussion

The findings of this study with our high-speed camera system were that RBC flows in single capillaries under physiological conditions were as high as 2 mm/s (Unekawa et al., 2008), and that flow was not stationary (Mchedlishvili, 1998), but rather high-frequency oscillatory in nature (capillary vasomotion). Employing two-photon microscopy, Kleinheld found that RBC flow in individual capillaries within the specific area sensitive to vibrissae was quite variable with a speed of 0.8 ± 0.5 mm/s and an oscillation frequency of 0.1 Hz in SD rats (Kleinfeld, 2002). When vibrissae were stimulated, the RBC velocity increase was limited to only a 20% increase over the basal velocity, which was comparable to the level of the highest fluctuations seen in single capillaries. According to Kleinfeld, flow increase would therefore be largely masked by basal fluctuations, limiting the sensitivity of brain imaging techniques, at least at low frequencies.

When neurons were depolarized during CSD and became dysfunctional, RBC flow became slower and was rectified, losing its oscillatory character, as described above. Periodic exclusion of RBCs was observed from the capillary network in association with on-going neuronal depolarization (Tomita et al., 2008b). This seems to conflict with the results of Takano et al., who found that CSD induced tissue hypoxia through a transient increase in oxygen demand; there was an increase in capillary flow for several minutes, followed by a relative decrease in mice (Takano et al., 2007b). It was also reported that CSD remarkably enhances CBF to support an increased metabolic rate (Piilgaard and Lauritzen, 2009; Shinohara et al., 1979) and induces mild initial hypoperfusion, followed by transient hyperemia (Ayata et al., 2004) in rats. However, our data are not necessarily in conflict with the above findings. In young rats, no increase in CBF was found in response to CSD, and accompanying transient capillary flow drop was observed, with cessation of RBC flux in 19% of capillaries (Chuquet et al., 2007). We found single capillaries in which RBC flow slowed in response to CSD, among the numerous capillaries examined in this study. We also preliminarily found single capillaries in which RBC flowed fast during the passage of CSD (unpublished data); namely, the flow response to CSD is not uniform.

Within a limited region, the existence of neuro-capillary coupling might be supported by the linear correlation between decrease in RBC

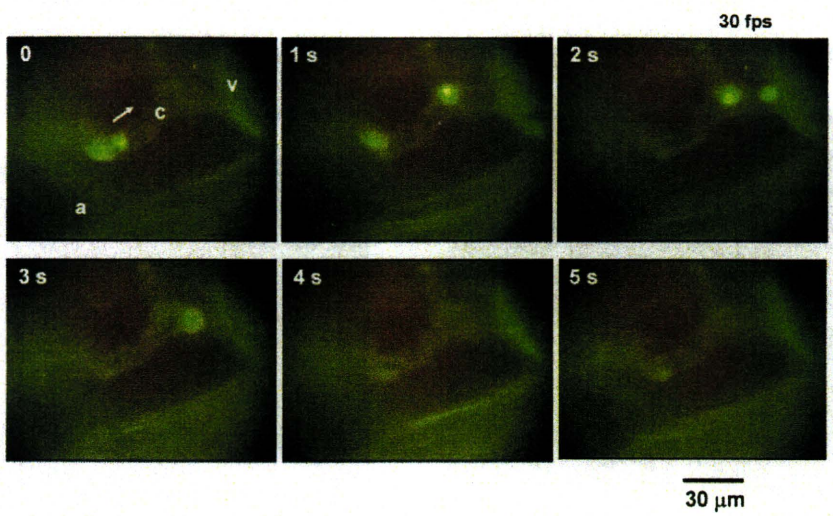

Fig. 13. FITC-labeled RBCs and FITC-stained endothelial cells, observed in a video clip (30 fps) at the peak of CSD (neuronal depolarization). The capillary plasma appeared to be very sludgy and viscous. In such sluggish flow, round RBCs in a single capillary (c) showed a staggering motion, occasionally coming to a full stop. On the other hand, flow in the arteriole and venule was quite well maintained in this case, as estimated from the elongation of flowing RBCs.

Please cite this article as: Tomita, M., et al., Oscillating neuro-capillary coupling during cortical spreading depression as observed by tracking of FITC-labeled RBCs in single capillaries, NeuroImage (2011), doi:10.1016/j.neuroimage.2011.02.078

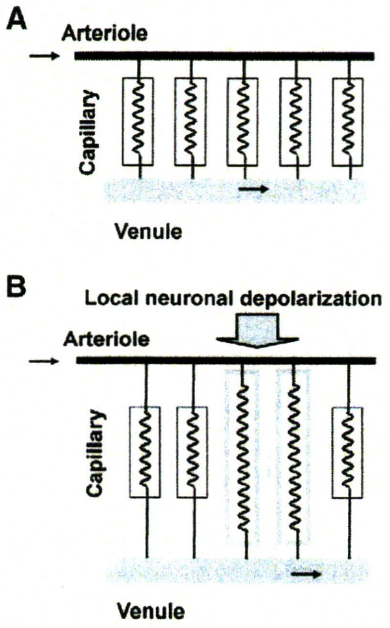

Fig. 14. A parallel capillary model. Top (A) equal resistance to capillary flow in the control state, bottom (B) during CSD, some capillary channels are involved in the propagating wave and the plasma in them becomes highly viscous. RBCs start to detour around the deranged channels.

velocity and change in tissue background darkness. In these circumstances, the flow would not follow Poiseuille's law, which states that the flow rate is proportional to the fourth power of the radius and inversely proportional to viscosity for a Newtonian fluid, and shear rate does not affect the viscosity. Rather, the flow would resemble that of a viscous non-Newtonian fluid, where shear rate does influence the viscosity. Systemic hemodilution increased RBC velocity and RBC flux in capillaries, probably due to reduced blood viscosity or lowered oxygen content. Thus, decrease in blood viscosity seems to be an important factor in the hyperemic response, possibly through a shear stress-dependent mechanism (Hudetz, 1997). Formation of spindle-shaped strings (Osada et al., 2006) or swelling of the neuronal cell body (Takano et al., 2007b) after elicitation of CSD might alter the shear stress in the nearby capillaries. Also, it was demonstrated that NO enhanced leukocyte rolling and modulated leukocyte–endothelial interaction (Lindauer et al., 1996). Locally produced NO might result in changes of local microcirculation, possibly through alteration of blood viscosity. In such cases, change in diameter of capillaries is no longer effective to regulate the flow (Mchedlishvili et al., 2000; Tomita, 2008). The decrease of RBC velocity in capillaries appears to be a local intrinsic event, since it occurs in the absence of any arterial blood pressure change and in the absence of observable diametric change in the upstream feeding arterial systems.

As shown in Fig. 14, RBC flows in all capillaries are regulated individually and independently (top A) in the control state, but when the neurons are depolarized during CSD (bottom B), some channels lose their regulation and the local capillary flow resistance is increased. Flowing RBCs would tend to be excluded from these high flow-resistance channels and would start to detour to other channels with lower flow-resistance.

Conclusions

The observed RBC flow behavior changes in intraparenchymal capillaries during CSD suggest the presence of a regulatory mechanism of cerebral capillary flow, presumably via hemorheological factors, that may involve a direct or indirect coupling between neurons and nearby capillaries via astroglial elements.

Supplementary data associated with this article can be found, in the online version, at doi:10.1016/j.neuroimage.2011.02.078.

The first author, Minoru Tomita, passed away on 17th January 2010. This work was completed by his co-authors.

Acknowledgments

This work was supported by JSPS Grants-in-Aid # 17390255 (Suzuki, N) and # 19591008 (Tomita, Y). The authors also thank Otsuka Pharmaceutical Co., Ltd. for financial support.

References

Anderson, T.R., Andrew, R.D., 2002. Spreading depression: imaging and blockade in the rat neocortical brain slice. J. Neurophysiol. 88, 2713–2725.
Ayata, C., Shin, H.K., Salomone, S., Ozdemir-Gursoy, Y., Boas, D.A., Dunn, A.K., Moskowitz, M.A., 2004. Pronounced hypoperfusion during spreading depression in mouse cortex. J. Cereb. Blood Flow Metab. 24, 1172–1182.
Biswal, B.B., Hudetz, A.G., 1996. Synchronous oscillations in cerebrocortical capillary red blood cell velocity after nitric oxide synthase inhibition. Microvasc. Res. 52, 1–12.
Chaigneau, E., Oheim, M., Audinat, E., Charpak, S., 2003. Two-photon imaging of capillary blood flow in olfactory bulb glomeruli. Proc. Natl. Acad. Sci. U. S. A. 100, 13081–13086.
Chuquet, J., Hollender, L., Nimchinsky, E.A., 2007. High-resolution in vivo imaging of the neurovascular unit during spreading depression. J. Neurosci. 27, 4036–4044.
del Zoppo, G.J., 2010. The neurovascular unit in the setting of stroke. J. Intern. Med. 267, 156–171.
Hudetz, A.G., 1997. Blood flow in the cerebral capillary network: a review emphasizing observations with intravital microscopy. Microcirculation 4, 233–252.
Kleinfeld, D., Mitra, P.P., Helmchen, F., Denk, W., 1998. Fluctuations and stimulus-induced changes in blood flow observed in individual capillaries in layers 2 through 4 of rat neocortex. Proc. Natl. Acad. Sci. U. S. A. 95, 15741–15746.
Kleinfeld, D., Denk, W., 2000. Two-photon imaging of neocortical microcirculation. In: Yuste, R., Lanni, F., Konnerth, A. (Eds.), Imaging Neurons: A Laboratory Manual. Cold Spring Harbor Laboratory Press, Cold Spring Harbor, pp. 23.10–23.15.
Kleinfeld, D., 2002. Cortical blood flow through individual capillaries in rat vibrissa S1 cortex: stimulus-induced changes in flow are comparable to the underlying fluctuations in flow. In: Tomita, M., Kanno, I., Hamel, E. (Eds.), Brain Activation and CBF Control; Exerpta Medica International Congress Series 1235. Elsevier Science, Amsterdam, pp. 115–122.
Krogh, A., 1919. The supply of oxygen to the tissues and the regulation of the capillary circulation. J. Physiol. 52, 457–474.
Leão, A., 1944. Spreading depression of activity in cerebral cortex. J. Neurophysiol. 7, 359–390.
Lindauer, U., Dreier, J., Angstwurm, K., Rubin, I., Villringer, A., Einhaupl, K.M., Dirnagl, U., 1996. Role of nitric oxide synthase inhibition in leukocyte–endothelium interaction in the rat pial microvasculature. J. Cereb. Blood Flow Metab. 16, 1143–1152.
Mchedlishvili, G., 1986. Arterial behavior and blood circulation in the brain. Plenum Press, New York.
Mchedlishvili, G., 1998. Disturbed blood flow structuring as critical factor of hemorheological disorders in microcirculation. Clin. Hemorheol. Microcirc. 19, 315–325.
Mchedlishvili, G., Tomita, M., Schmid-Sconbein, G.W., 2000. Hemorrheology in microcirculation: pathological changes. Internet Virtual Symposium, the 7th Tbilisi Symposium. Keio J. Med., 49 (Suppl. 3). Keio University, Tokyo.
Nakai, K., Imai, H., Kamei, I., Itakura, T., Komari, N., Kimura, H., Nagai, T., Maeda, T., 1981. Microangioarchitecture of rat parietal cortex with special reference to vascular "sphincters." Scanning electron microscopic and dark field microscopic study. Stroke 12, 653–659.
Nimmerjahn, A., Kirchhoff, F., Kerr, J.N., Helmchen, F., 2004. Sulforhodamine 101 as a specific marker of astroglia in the neocortex in vivo. Nat. Methods 1, 31–37.
Osada, T., Tomita, M., Suzuki, N., 2006. Spindle-shaped constriction and propagated dilation of arterioles during cortical spreading depression. NeuroReport 17, 1365–1368.
Piilgaard, H., Lauritzen, M., 2009. Persistent increase in oxygen consumption and impaired neurovascular coupling after spreading depression in rat neocortex. J. Cereb. Blood Flow Metab. 29, 1517–1527.
Schiszler, I., Tomita, M., Fukuuchi, Y., Tanahashi, N., Inoue, K., 2000. New optical method for analyzing cortical blood flow heterogeneity in small animals: validation of the method. Am. J. Physiol. 279, H1291–H1298.
Seylaz, J., Charbonné, R., Nanri, K., Von Euw, D., Borredon, J., Kacem, K., Méric, P., Pinard, E., 1999. Dynamic in vivo measurement of erythrocyte velocity and flow in capillaries and of microvessel diameter in the rat brain by confocal laser microscopy. J. Cereb. Blood Flow Metab. 19, 863–870.
Shinohara, M., Dollinger, B., Brown, G., Rapoport, S., Sokoloff, L., 1979. Cerebral glucose utilization: local changes during and after recovery from spreading cortical depression. Science 203, 188–190.
Takano, T., Han, X., Deane, R., Zlokovic, B., Nedergaard, M., 2007a. Two-photon imaging of astrocytic Ca^{2+} signaling and the microvasculature in experimental mice models of Alzheimer's disease. Ann. NY Acad. Sci. 1097, 40–50.

Takano, T., Tian, G.F., Peng, W., Lou, N., Lovatt, D., Hansen, A.J., Kasischke, K.A., Nedergaard, M., 2007b. Cortical spreading depression causes and coincides with tissue hypoxia. Nat. Neurosci. 10, 754–762.

Tomita, M., Gotoh, F., Sato, T., Tanahashi, N., Tanaka, K., 1981. 4–6 Cycle per minute fluctuation in cerebral blood volume of feline cortical tissue in situ. J. Cereb. Blood Flow Metab. 1 (Suppl 1), S443–S444.

Tomita, M., Fukuuchi, Y., Terakawa, S., 1994. No appreciable swelling of cultured neurons after oxygen deprivation, and cell damage occasionally aggravated by oxygen resupply. In: Hartmann, A., Yatsu, Y., Kuschinsky, W. (Eds.), Cerebral Ischemia and Basic Mechanisms. Springer-Verlag, Berlin Heidelberg, pp. 273–280.

Tomita, M., Schiszler, I., Tomita, Y., Tanahashi, N., Takeda, H., Osada, T., Suzuki, N., 2005a. Initial oligemia with capillary flow stop followed by hyperemia during K^+-induced cortical spreading depression in rats. J. Cereb. Blood Flow Metab. 25, 742–747.

Tomita, M., 2008. Basic mechanisms of brain ischemia; minireview on microcirculation capillo-venous flow disturbances in brain ischemia. In: Erdő, F. (Ed.), Recent Advances and New Strategies in Stroke Research. Transworld Research Network, Kerala, India, pp. 91–112.

Tomita, M., Osada, T., Schiszler, I., Tomita, Y., Unekawa, M., Toriumi, H., Tanahashi, N., Suzuki, N., 2008a. Automated method for tracking vast numbers of FITC-labeled RBCs in microvessels of rat brain in vivo using a high-speed confocal microscope system. Microcirculation 15, 163–174.

Tomita, M., Tomita, Y., Osada, T., Unekawa, M., Toriumi, H., Tatarishvili, J., Suzuki, N., 2008b. Periodic disappearance of RBC from focal capillary network during K^+-induced cortical spreading depression in rodents. J. Vasc. Res. 45 (Suppl. 2), 65.

Tomita, M., Osada, T., Unekawa, M., Tomita, Y., Toriumi, H., Suzuki, N., 2009a. Exogenous nitric oxide increases microflow but decreases RBC attendance in single capillaries in rat cerebral cortex. Microvasc. Rev. Commun. 3, 11–16.

Tomita, M., Tomita, Y., Toriumi, H., Unekawa, M., Suzuki, N., 2009b. Coupling of capillary RBC flow failure with neuronal depolarization. Nature Proceedings. The data are available at http://precedings.nature.com/documents/3220/version/1.

Tomita, Y., Tomita, M., Schiszler, I., Amano, T., Tanahashi, N., Kobari, M., Takeda, H., Ohtomo, M., Fukuuchi, Y., 2002. Repetitive concentric wave-ring spread of oligemia/hyperemia in the sensorimotor cortex accompanying K^+-induced spreading depression in rats and cats. Neurosci. Lett. 322, 157–160.

Tomita, Y., Kubis, N., Calando, Y., Tran Dinh, A., Méric, P., Seylaz, J., Pinard, E., 2005b. Long-term in vivo investigation of mouse cerebral microcirculation by fluorescence confocal microscopy in the area of focal ischemia. J. Cereb. Blood Flow Metab. 25, 858–867.

Unekawa, M., Tomita, M., Osada, T., Tomita, Y., Toriumi, H., Tatarishvili, J., Suzuki, N., 2008. Frequency distribution function of red blood cell velocities in single capillaries of the rat cerebral cortex using intravital laser-scanning confocal microscopy with high-speed camera. Asian Biomed. 2, 203–218.

Unekawa, M., Tomita, M., Tomita, Y., Toriumi, H., Hattori, H., Suzuki, N., 2009. Shift of frequency distribution of RBC velocity in parenchymal capillaries during potassium-induced cortical spreading depression in rats. J. Cereb. Blood Flow Metab. 29, S298.

Unekawa, M., Tomita, M., Tomita, Y., Toriumi, H., Miyaki, K., Suzuki, N., 2010. RBC velocities in single capillaries of mouse and rat brains are the same, despite 10-fold difference in body size. Brain Res. 1320, 69–73.

Villringer, A., Them, A., Lindauer, U., Einhäupl, K., Dirnagl, U., 1994. Capillary perfusion of the rat brain cortex. An in vivo confocal microscopy study. Circ. Res. 75, 55–62.

Vogel, J., Abounader, R., Schrock, H., Zeller, K., Duelli, R., Kuschinsky, W., 1996. Parallel changes of blood flow and heterogeneity of capillary plasma perfusion in rat brains during hypocapnia. Am. J. Physiol. 270, H1441–H1445.

Wolf, J., 1970. Anchorage of collagenous fibrils in brain surface wrapping basal membrane (membrana limitans gliae superficialis). Folia Morphol. Praha 18, 322–329.

Yanamoto, K., Hosoi, R., Uesaka, Y., Abe, K., Tsukada, H., Inoue, O., 2003. Intrastriatal microinjection of sodium nitroprusside induces cell death and reduces binding of dopaminergic receptors. Synapse 50, 137–143.

Please cite this article as: Tomita, M., et al., Oscillating neuro-capillary coupling during cortical spreading depression as observed by tracking of FITC-labeled RBCs in single capillaries, NeuroImage (2011), doi:10.1016/j.neuroimage.2011.02.078